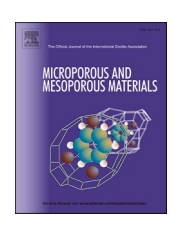
ELSEVIER

Contents lists available at ScienceDirect

Microporous and Mesoporous Materials

journal homepage: www.elsevier.com/locate/micromeso





Operando infrared spectroscopy to probe the importance of framework selection in silicon-doped aluminophosphates, SAPO-5, SAPO-11, SAPO-18, and SAPO-34, for acid catalysed dimethyl ether formation

M.G. Walerowski^a, A.E. Oakley^a, M. Carravetta^a, R. Raja^a, L.M. Armstrong^b, M.E. Potter^{c,d,*}

- ^a School of Chemistry and Chemical Engineering, University of Southampton, Southampton, SO17 1BJ, UK
- ^b School of Engineering, University of Southampton, Southampton, SO17 1BJ, UK
- ^c Institute of Sustainability and Climate Change, Department of Chemistry, University of Bath, Bath, BA2 7AY, UK
- ^d UK Catalysis Hub, Research Complex at Harwell (RCaH), Harwell, Didcot, OX11 0FA, UK

ARTICLE INFO

Keywords: Zeolite SAPO Catalysis Acid Infrared Spectroscopy Operando

ABSTRACT

Methanol dehydration chemistry is heavily reliant on solid acid catalysts for the formation of a wide range of hydrocarbons. Whilst olefins are routinely formed on strong Brønsted acid sites, there is a growing interest in dimethyl ether production, due to its potential as a sustainable fuel alternative, which is compatible with current petroleum infrastructure. The effective formation of dimethyl ether over extended time periods typically favours weaker acid sites. Here, two methanol molecules can couple together, reducing the formation of larger aromatic products that facilitate the methanol-to-olefin process, but which can also facilitate catalyst deactivation. In this manuscript, we use *operando* diffuse reflectance infrared Fourier transform spectroscopy to probe methanol dehydration on a range of microporous silicon-doped aluminophosphates (SAPO-5, SAPO-11, SAPO-18, and SAPO-34), correlating the findings with catalytic data to highlight the key parameters for an effective methanol-to-dimethyl ether catalyst. In doing so, we demonstrate that weaker acid sites play a key role in the production of dimethyl ether by permitting bound methoxy species and unbound methanol molecules to co-exist, triggering dimethyl ether formation.

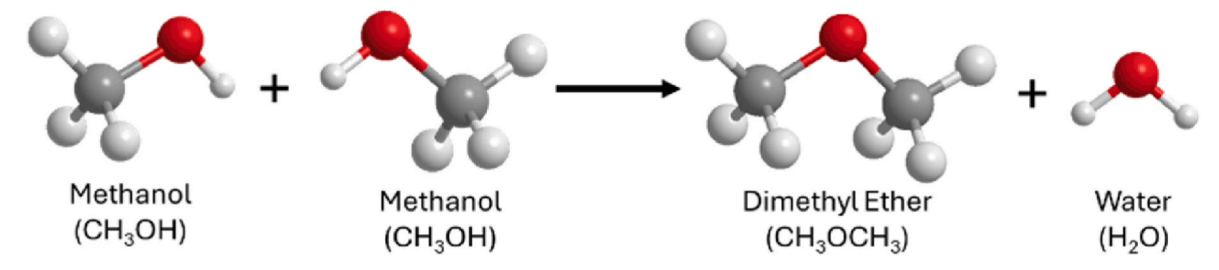
1. Introduction

Dimethyl ether (DME) is a simple, non-toxic, alternative fuel with a high cetane number which could be sustainably-produced via a circular carbon economy, and thus support defossilisation of the transport sector [1–3]. As DME is compatible with existing liquid petroleum gas infrastructure owing to their similar physicochemical properties [1,2], it could be readily deployed as a short-to-medium term solution for achieving ambitious climate goals. Traditionally, DME has been produced via the bimolecular dehydration of methanol with solid acid catalysts (Scheme 1) [1–3]. γ -Al₂O₃ can selectively dehydrate methanol-to-DME due to its weakly acidic Lewis sites, but it can suffer from rapid water-induced deactivation, limiting its use for this reaction [3–5]. In contrast, microporous solid acid catalysts, such as the zeolite H-ZSM-5, are less susceptible to deactivation by water [6]. Additionally, confinement effects conferred by the microporous topology may decrease activation barriers [7], and improve catalytic activity. Zeolites

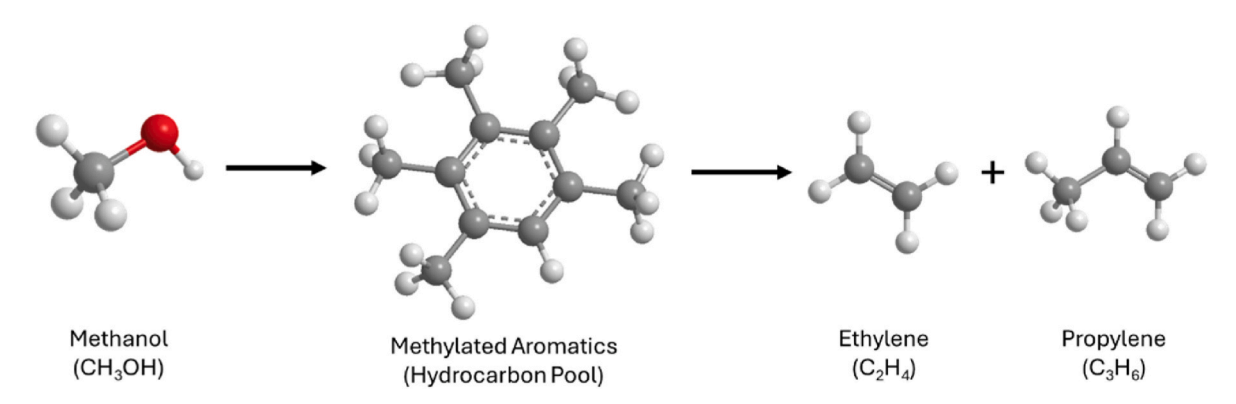
however often contain strong Brønsted acid sites (BAS), which may dehydrate methanol to olefinic products and/or coke precursors. This can have a detrimental effect on both DME selectivity and catalyst longevity, as coke build-up within the microporous framework may restrict access to internal acid sites [1,5,8,9].

Aluminophosphates (AlPOs) have frameworks analogous to zeolites, however AlPO frameworks are constructed from vertex-sharing AlO₄ and PO₄ tetrahedra in contrast to vertex-sharing SiO₄ and AlO₄ tetrahedra in zeolites [10]. Isomorphous substitution of silicon into the AlPO framework can generate charge-balancing BAS [11,12], which can catalyse the dehydration of methanol-to-DME. The properties of the BAS formed vary with the framework and the substitution mechanism. Silicon can substitute into the AlPO framework by replacing either a framework phosphorus atom (type II) to create an isolated BAS or replace adjacent aluminium-phosphorous pairs (type III) to yield silicon islands (Fig. S1). The type III mechanism decreases the number of acid sites formed per silicon atom as BAS are only formed on the periphery of

^{*} Corresponding author. Institute of Sustainability and Climate Change, Department of Chemistry, University of Bath, BA2 7AY, UK. *E-mail address:* mep61@bath.ac.uk (M.E. Potter).



Scheme 1. Bimolecular dehydrative coupling of methanol to give DME.



Scheme 2. Showing the role of aromatic molecules in forming a hydrocarbon pool, which facilitate the formation of olefins in MTO chemistry.

these neutral silicon islands [10,11].

Numerous investigations have focused on understanding the precise structure of SAPOs, and their catalytic performance during methanol dehydration. Several studies have reported that SAPOs possess substantial diversity with regards to their acid site strength and abundance, with SAPO-5 and SAPO-11 often exhibiting weaker and less abundant acid sites compared to SAPO-18 and SAPO-34 [11-14]. Computational modelling studies have indicated that acid site strength and location affect the reaction mechanism, activation barriers, and hence the catalytic performance of SAPOs during methanol dehydration [15,16]. You et al. experimentally demonstrated that SAPO-18 and SAPO-34 show high initial methanol dehydration activity, but deactivate rapidly due to significant coke build-up. Possibly this was due to the stronger BAS initiating the formation of coke precursors such as methylated (poly-) aromatic molecules, associated with the hydrocarbon pool in MTO (methanol-to-olefin) processes (Scheme 2). In contrast, SAPO-5 and SAPO-11 with weaker and less abundant acid sites showed lower, albeit more stable, catalytic activity [14]. Similar studies have reported largely the same findings, that SAPOs with more abundant and stronger acid sites tend to show higher initial activity, but deactivate rapidly with time-on-stream due to coke build up within the internal porosity, showing the importance of pore topology also [10,12,13,17].

In situ and operando techniques can provide a deeper insight into methanol dehydration over SAPOs and zeolites. Using in situ FT-IR (Fourier transform infrared) spectroscopy, Schnabel et al. found that bands attributed to coke start appearing at temperatures as low as 220 °C during methanol dehydration over SAPO-34 [18]. The in situ IR spectra for SAPO-11 were comparable to SAPO-34, suggesting that methanol dehydration followed similar mechanistic pathways over both catalysts. However, the intensity of all IR bands was lower for SAPO-11, which could be attributed to weaker and less abundant BAS. Lin et al. studied the MTO reaction over H-ZSM-5 using a variety of techniques, such as in situ DRIFTS (diffuse reflectance infrared Fourier transform spectroscopy) and NMR (nuclear magnetic resonance) [19]. They found that the formation of crucial surface methoxy intermediate species from methanol over H-ZSM-5 was relatively sluggish, compared to formation of methoxy species from DME. They hypothesised that methanol would

be stabilised through dimer or cluster formation, whereas DME was less polar and would not stabilise to the same extent. Using in situ UV-Vis, Dai et al. found that SAPO-11, SAPO-34, and SAPO-41 were all capable of forming a hydrocarbon pool (HCP) which is crucial for the MTO reaction. The intensity of these peaks however varied between the catalysts, with SAPO-11 showing weaker bands [20]. Similarly, Borodina et al. and Goetze et al. used operando UV-Vis to demonstrate that the precise framework topology and reaction parameters can influence the mechanistic pathway and catalytic performance [21,22]. Herein, we performed an extensive study to explore the influence of both the framework and operating conditions on the methanol to DME reaction over a range of SAPO solid acid catalysts. By combining a suite of ex situ, operando, and post factum characterisation techniques, we were able to develop a holistic understanding of structural and mechanistic pathways which contribute to high activity, selectivity, and stability during methanol dehydration over SAPO-5, SAPO-11, SAPO-18, and SAPO-34 solid acid catalysts. These catalysts were chosen to represent a range of framework topologies, including larger one-dimensional channels in SAPO-5 (AFI framework, 7.3 $\text{Å} \times 7.3 \, \text{Å}$), medium sized one-dimensional channels in SAPO-11 (6.5 $\mbox{\normalfont\AA}\ \times\ 4.0$ $\mbox{\normalfont\AA}\)$, and three-dimensional cage structures of SAPO-18 (AEI, 3.8 Å imes 3.8 Å) and SAPO-34 (CHA, 3.8 Å imes3.8 Å). With this variety of frameworks, we will probe the mechanisms behind methanol-to-DME, and MTO chemistry.

2. Experimental

2.1. Catalyst synthesis

All four catalysts were synthesised using hydrothermal methods, in a sealed Teflon-lined Parr reactor. Brief details are provided below, with further details located in the supplementary information.

SAPO-5 was synthesised by mixing pseudo boehmite (Al source), phosphoric acid (P source), Ludox AS-40 (Si source), triethylamine (TEA, templating agent), and deionised water to make a gel with the ratio: 1.0Al:1.4P:0.3Si:1.4TEA:34H₂O. The gel was crystallised at 200 °C, for 24 h, under 500 rpm of stirring. The solid was then filtered, dried, and calcined under a flow of air at 600 °C, with a 2.5 °C min⁻¹

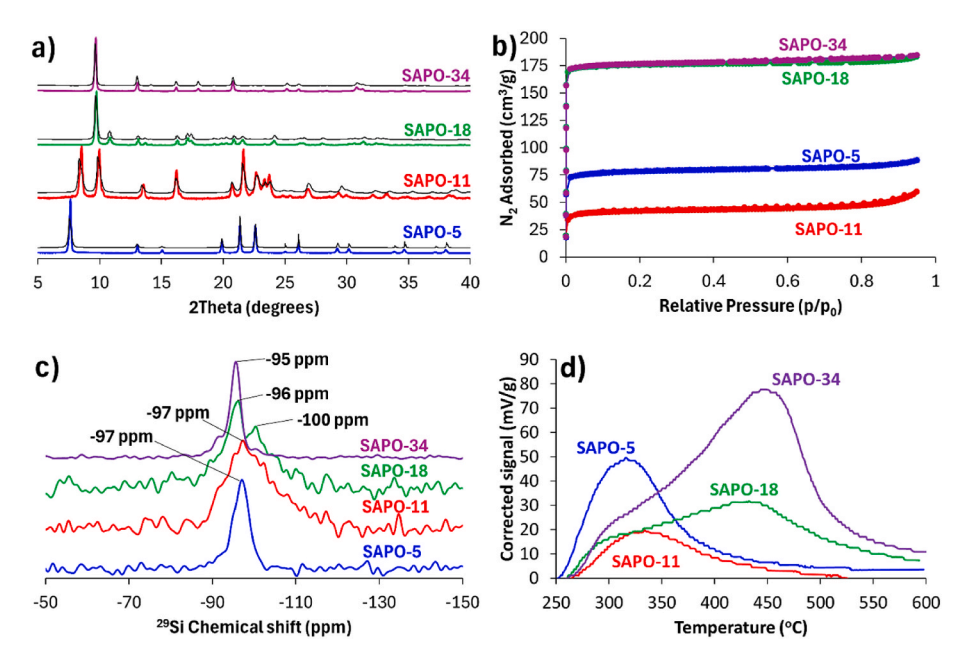


Fig. 1. Characterisation data of the four SAPO catalysts, showing: a) phase purity by comparing the experimental powder XRD patterns against ideal XRD patterns calculated bases on ideal CIF files, b) typical type I adsorption isotherms from N₂ physisorption, c) silicon environments through ²⁹Si ssNMR, and d) acid strength distribution through NH₃-TPD. (For interpretation of the references to colour in this figure legend, the reader is referred to the Web version of this article.)

ramp rate, for 24 h.

SAPO-11 was synthesised by mixing aluminium isopropoxide (Al source), phosphoric acid (P source), Ludox AS-40 (Si source), diisopropylamine (DPA, templating agent), and deionised water to make a gel with the ratio: 1:0Al:1.0P:0.2Si:1.0DPA:25H₂O. The gel was crystalised at 200 $^{\circ}$ C, for 48 h, with no stirring. The solid was then filtered, dried, and calcined under a flow of air at 600 $^{\circ}$ C, with a 2.5 $^{\circ}$ C min⁻¹ ramp rate, for 40 h.

SAPO-18 was synthesised by mixing aluminium hydroxide (Al source), phosphoric acid (P source), fumed silica (Si source), N,N-diisopropylethylamine (DPEA, templating agent), and deionised water to make a gel with the ratio: 1:0Al:0.9P:0.2Si:0.8DPEA:25H₂O. The gel was crystalised at 160 °C, for 192 h, with no stirring. The solid was then filtered, dried, and calcined under a flow of air at 600 °C, with a 2.5 °C min $^{-1}$ ramp rate, for 16 h.

SAPO-34 was synthesised by mixing aluminium isopropoxide (Al source), phosphoric acid (P source), fumed silica (Si source), tetraethylammonium hydroxide (TEAOH, templating agent), and deionised water to make a gel with the ratio: 1.0Al:1.0P:0.15Si:1.0TEAOH:9H $_2$ O. The gel was crystallised at 200 °C for 72 h, with no stirring. The solid was then filtered, dried, and calcined under a flow of air at 600 °C, with a 2.5 °C min $^{-1}$ ramp rate, for 16 h.

2.2. Physicochemical characterisation

Brief descriptions of the characterisation protocols are provided below, with further details outlined in the supplementary information:

Powder X-ray diffraction (PXRD) was performed using a Bruker D2 Phaser with Cu Kα radiation.

Nitrogen physisorption (BET) was performed using a Micrometrics Tristar II 3020 analyser at 77 K. Catalysts were dried under vacuum at $120~^{\circ}$ C prior to measuring, after which 124 adsorption, and 30 desorption points were collected between relative pressures of 0.00 and 0.95.

Scanning electron microscopy (SEM) was performed on a JEOL JSM-7200F, without sputter coating, with a 5 kV acceleration voltage and a 93 μ A emission current.

Inductively coupled plasma – optical emission spectroscopy (ICP-OES) was performed commercially by MEDAC Ltd.

Solid state nuclear magnetic resonance (ssNMR) was performed

on dried catalysts on a Agilent Varian 600 MHz Premium Shielded spectrometer with a 14.1 T field strength. For 27 Al and 31 P spectra the rotors were spun at 14,000 Hz, at the magic angle and spectra acquired in triple (1 H- 27 Al- 31 P) resonance mode. Both 27 Al and 31 P spectra were collected over 128 scans. For 29 Si spectra the spectra were collected in cross polarisation mode, over 4096 scans.

Ammonia temperature programmed desorption (NH₃-TPD) was performed on a Quantachrome ChemBET Pulsar TPR/TPD instrument. 200 mg of catalyst was dried at 550 °C under a 20 % O₂ flow. The catalyst was then exposed to 5 % NH₃ at 150 °C for 2 h, and then heated to 600 °C under He at a ramp rate of 5 °C min⁻¹, and then held for 1 h, whilst the outlet gases were measured using a thermal conductivity detector.

Thermogravimetric analysis (TGA) was performed using a TA instruments TGA 5500, where catalysts were heated from 30 to 700 $^{\circ}$ C, at 10 $^{\circ}$ C min⁻¹ under 25 mL min⁻¹ of air.

UV–Vis was performed using a Perkin Elmer UV–Vis/NIR Lambda 750s spectrometer with a 100 mm integrating sphere, in diffuse reflectance mode.

2.3. Catalysis protocol

0.300~g of sieved SAPO catalyst (300–500 μm) was activated at 400 $^{\circ} C$ in a 25 mL min $^{-1}$ flow of nitrogen for 1 h. The reactor was then cooled to reaction temperature before 18.96 μL min $^{-1}$ of methanol (WHSV of $3.00~hr^{-1}$) was passed into the reactor in a 25 mL min $^{-1}$ flow of nitrogen carrier gas. The outlet vapour was mixed with a 18.96 μL min $^{-1}$ flow of chloroform, which served as the external standard. 0.2 mL samples were taken from this flask for manual injection into a Perkin Elmer Clarus 480 gas chromatograph (GC) for analysis. Outlet gas was analysed in triplicate, reactor temperature was then increased by 15 $^{\circ} C$ and the process repeated. Mass balances were calculated using the chloroform external standard, using GC response factors, experimentally determined by our own calibrations. In all cases, the mass balances were found to be between 97 and 103 mol%. For the time-on-stream stability study, the temperature and methanol WHSV were held at 275 $^{\circ} C$ and 3 h^{-1} throughout the study to accelerate catalyst deactivation.

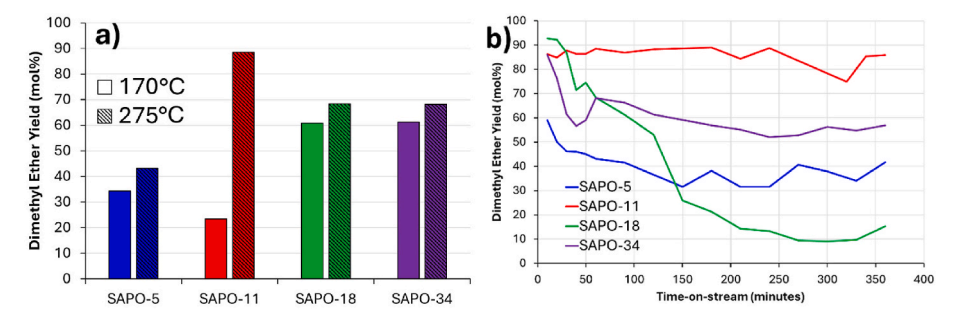


Fig. 2. Catalytic methanol dehydration to DME data showing variation in DME yield as a function of a) reaction temperature after 1 h on-stream and b) time-on-stream. Conditions: 275 $^{\circ}$ C (or as stated), 0.300 g of catalyst (300–500 μm sieve fraction), nitrogen flow of 25 mL min⁻¹, methanol flow of 18.96 μL min⁻¹ (equivalent to methanol WHSV of 3.00 hr⁻¹).

2.4. DRIFTS procedure

Diffuse reflectance infrared Fourier transform spectroscopy (DRIFTS) was performed in a Harrick high temperature DRIFTS cell fitted with ZnSe windows. The cell was attached to the Praying Mantis Optics and spectra collected with an Agilent Carey 680 FTIR spectrometer.

50 mg of the SAPO catalyst was loaded into the system and 30 mL min⁻¹ of N₂ was flown through the system, which was heated to 80 °C, at a ramp rate of 10 °C min⁻¹ and held for 1 h, without the chiller on, to dehydrate the cell itself. The nitrogen was kept running at this flow rate throughout the whole experiment. After this, the chiller was turned on and the system ramped up to 400 °C at a rate of 10 °C min⁻¹ and held for 1 h to dry the catalyst. After 1 h, a spectrum was collected. The system was then cooled down to 30 °C at a rate of 20 °C min⁻¹. A scan was then taken once at 30 °C. 1 µL of methanol was injected into the inlet, and after 1 min a spectrum was collected. 5 min after the injection another 1 μL was added until a total of 7 μL had been injected, at which point the system was left to equilibrate for 10 min and a spectrum collected. The system was ramped to 400 °C at a rate of 5 °C min⁻¹, with spectra collected at 50 °C and then every 25 °C after this until 400 °C, at which point the system was cooled to 30 °C and a final spectrum collected. All spectra are the sum of 128 scans, and are presented in absorbance inkeeping with our previous work [23].

The outlet gas was monitored using a Hiden Analytical Quantitative Gas Analyser, following m/z signals of 18 (water), 28 (nitrogen), 31 (methanol), 45 (dimethyl ether), ethene (27), and propene (41).

3. Results and discussion

3.1. Catalyst integrity

The four microporous SAPO catalysts (SAPO-5, SAPO-11, SAPO-18, and SAPO-34), were individually synthesised using hydrothermal procedures. The integrity of the resulting calcined white powders was evidenced using an array of characterisation techniques. Powder X-ray diffraction (PXRD, Fig. 1a) showed that only peaks attributed to the intended (theoretical) framework were present in the experimental PXRD patterns, indicating phase purity. Some catalysts showed subtle shifts in peak positions compared to the theoretical values [24-27] and previously reported patterns [28–30]. This is likely caused by variations in sample height in the bench-top diffractometers, or potentially marginal variations in unit cell parameters (Table S1). SEM images show uniform particle sizes, with the SAPO-5 showing small hexagonal particles, SAPO-11 showing intergrowths, and SAPO-18 and SAPO-34 showing cubic particles, as expected (Fig. S2). Nitrogen physisorption probed the porosity of the catalysts (Fig. 1b), and in all cases presented a typical type I adsorption isotherm as expected for microporous materials. Surface areas and pore volumes were found to be in good agreement with previously published results for these catalysts (Table S2)

[28-30].

Inductively coupled plasma (ICP) analysis demonstrated a variation in silicon loading between the four catalysts, ranging from 2.5 to 3.7 wt % (Table S2). To probe the atomic environment, solid state nuclear magnetic resonance (ssNMR, Fig. 1c & S3) measurements were performed on the framework ²⁷Al and ³¹P nuclei, whilst cross-polarisation measurements probed the dopant ²⁹Si nuclei. In all cases, the ²⁷Al spectra (Fig. S3a) showed a single peak at 37 ppm, indicative of framework tetrahedral AlO₄ species, with no signs of defect AlO₅ species, or extra framework AlO₆ species [31]. Similarly, the ³¹P spectra (Fig. S3b) showed a single peak between -32 and -30 ppm, attributed to the expected tetrahedral PO₄ species [31]. Comparing the ²⁹Si spectra (Fig. 1c) gives information on the environment of the doped Si nuclei, and therefore the associated acid sites. The variation in the signal-to-noise ratio between the four SAPOs is attributed to both the spread of environments, and the different packing densities of the four catalysts. SAPO-34 shows a primary peak at -95 ppm associated with the Si(OAl)₃(OHAl) environment, due to silicon substituting a framework phosphorus atom [32,33]. SAPO-5 and SAPO-11 show a slight downshift in ppm, suggesting comparatively fewer isolated sites, and a greater fraction of Si-O-Si linkages. SAPO-18 shows a separate secondary peak at -101 ppm, clearly indicating Si-O-Si linkages, due to silicon islanding [34]. Unlike SAPO-5 and SAPO-34, SAPO-11 shows a very broad signal, likely due to a range of silicon environments, suggesting varying degrees of silicon islanding.

Ammonia temperature programmed desorption (NH3-TPD, Fig. 1d) was used to probe the strength and quantity of acid sites in the four SAPO systems. The data showed two distinct acid sites, weaker acid sites with maxima between 300 and 350 °C, and stronger acid sites with maxima between 400 and 450 °C. SAPO-34 has the greatest quantity of acid sites, in line with having the greatest silicon loading and a higher proportion of isolated silicon sites forming BAS. Furthermore, these acid sites were primarily stronger acid sites, as expected for SAPO-34. SAPO-18 and SAPO-5 had comparable quantities of acid sites (Table S3), likely due to differing silicon substitution mechanisms, where SAPO-18 showed significantly more islanding, lowering the number of possible active sites. SAPO-18 possessed mainly stronger acid sites, whereas SAPO-5 possessed weaker acid sites. Finally, SAPO-11 had the smallest number of acid sites, which were mainly weaker acid sites. The lower number of acid sites in SAPO-11 is likely a combination of the lower silicon loading, and the broader distribution of silicon environments which suggest substantial silicon islanding (as seen in the ssNMR) [11–14]. Silicon islanding causes a deviation from the one silicon atom forming one acid site relationship, which vindicates the low number of total acid sites observed.

3.2. Catalytic performance

The catalytic activity of the SAPOs was compared for converting methanol to DME (Fig. 2). It is noted that at 170 $^{\rm o}$ C, DME was the

Table 1Experimental DRIFTS assignments.

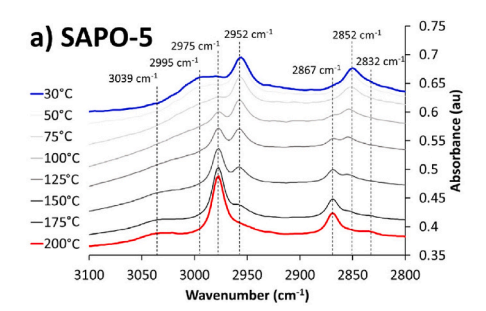
Peak position (cm ⁻¹)				Assignment
SAPO- 5	SAPO- 11	SAPO- 18	SAPO- 34	
3741	3739	3739	3742	Silanol Si-OH groups [42]
3670	3677	3671	3673	Defect Al-OH groups [42]
3613	3615	3615	3619	Al-OH-Si BAS hydrogen bonded [40, 41]
3517	3525	3592	3598	Al-OH-Si BAS less hydrogen bonding [40,41]
3594	3604	3590	3584	Confined methanol [43–46]
3039		3033	3032	Protonated DME [44]
2995	3005	3002	3004	H-bonded methanol [44]
2975	2975	2975	2975	Methoxy [44]
2952	2954	2954	2954	H-bonded methanol [44]
2867	2867	2865	2865	Methoxy [44]
2852	2846	2852	2846	H-bonded methanol [44]
2832	2832	2832	2836	H-bonded DME [44]

primary product, with selectivity above 99 mol%, with only traces of other products observed. As such, in this temperature regime the conversion and yield were equivalent. At the lower temperature of 170 °C (Fig. 2a) the DME yield increased with the number of strong acid sites, with SAPO-34 and SAPO-18 having the highest number of strong acid sites, with similar activity (both 61 mol% DME yield), followed by SAPO-5 (34 mol%), and finally SAPO-11 (23 mol%). As temperature increased to 275 °C, the DME yield of all systems increased (Fig. 2a). SAPO-11 showed a significant increase in yield as the conversion increased from 23 to 89 mol%, whilst retaining a DME selectivity of over 99 mol%. In contrast, the more modest increases in DME yield for SAPO-5, SAPO-18, and SAPO-34 can be rationalised by the fact that an increase in methanol conversion was countered by a reduction in DME selectivity. This is due to SAPO-5, SAPO-18, and SAPO-34 beginning to form short chain alkenes (ethene, propene, and butenes) at 275 °C, as the alternative MTO pathway occurs [35,36]. However, the acid sites in SAPO-11 are likely too few and too weak to initiate the competing MTO process, leading to a consistently high DME selectivity, as observed in our previous work [37]. The performance of the catalysts at 275 °C was monitored over several hours to explore their stability (Fig. 2b & S4). After 6 h on-stream, the SAPO-11 DME yield remained largely unchanged, whilst all other systems (SAPO-5, SAPO-18, and SAPO-34) showed a significant decrease in DME yield. To gain a greater understanding of this phenomenon, thermogravimetric analysis was performed on the catalysts after the time-on-stream study (Fig. S5). The mass of SAPO-34 and SAPO-18 decreased by 19 and 18 wt%, respectively. SAPO-5 decreased by 7 wt%, whilst SAPO-11 only decreased by 2 wt%. These TGA mass decreases correlate well with the number of strong acid sites seen using NH3-TPD, and the decrease in catalytic activity. Here, SAPO catalysts with a greater number of stronger acid sites likely accumulate more organic coke, leading to a greater reduction in activity. This is supported by the UV-Vis spectra of the spent catalysts (Fig. S6), which indicates that in SAPO-5, SAPO-18, and SAPO-34, polyaromatic and polyalkylated aromatic species form as indicated by a band centred at 400 nm. This is in good agreement with MTO literature [9], where it is proposed that stronger sites are needed to initiate the MTO reaction and promote the HCP mechanism. After the initial formation of short chain olefins (ethene and propene), bulky aromatic products form in the internal porosity of microporous frameworks, as has been previously shown in a range of studies [38,39]. In contrast, the UV-Vis spectrum of SAPO-11 does not show bands attributable to these polyaromatic and polyalkylated aromatic species, suggesting that the acid sites in SAPO-11 are too weak and too few to facilitate the MTO reaction pathway, thus limiting the formation of olefinic products and coke-precursors which vindicates the excellent DME selectivity and stability of SAPO-11.

3.3. Operando DRIFTS

To gain a greater insight into the mechanistic pathway of methanol dehydration in the four SAPO catalysts, operando DRIFTS was performed. The dried SAPO catalysts showed subtle variations as expected (Fig. S7). SAPO-5 presented a prominent feature at 3517 cm⁻¹, previously attributed to hydrogen-bonded (interacting with neighbouring framework oxygens) framework BAS, with a second signal at 3625 cm⁻¹ attributed to non-hydrogen bonded species (Table 1) [40]. Similarly, SAPO-11 also presented a broad signal at 3525 cm⁻¹ and a narrower signal at 3620 cm⁻¹, again assigned to hydrogen bonded, and BAS sites with less (or no) hydrogen bonding, respectively. In contrast, SAPO-18 and SAPO-34 showed two overlapping signals at 3598 and 3625 cm⁻¹ which are typical of their topology, and are likely due to the BAS residing in different rings or channels of the similar CHA and AEI framework topologies [41]. All spectra showed signals at roughly 3670 and 3740 cm⁻¹, which have previously been assigned to defect Al-OH and silanol (Si-OH) species, respectively [42]. On dosing with methanol (Fig. 3 & S8), the two BAS signals in SAPO-5 were replaced with a signal at 3594 cm⁻¹, which has previously been attributed to the O-H stretch of methanol residing within a porous framework. As expected, the SAPO-5 BAS signals shifted to a lower wavenumber on interacting with the methanol hydroxy group, and present as a broad band between 3100 and 3400 cm⁻¹ [43–46].

Focussing on the C-H region (3100–2800 cm⁻¹, Fig. 3a), new signals appeared on adsorbing methanol, a broad feature at 2995, and more pronounced features at 2956 and 2852 cm⁻¹. These latter two features are attributed to C-H stretches of strongly bound methanol (Table 1), whereas the broader feature at 2995 cm⁻¹ is likely weakly bound methanol, suggesting a range of methanolic species are concurrently present in the catalyst [43–46]. Heating the system from 30 to 100 °C showed a notable decrease in the 2995 cm⁻¹ feature, supporting this assignment as weakly bound methanol, which had likely desorbed, or transformed into more strongly-bound species [47]. The C-H stretches



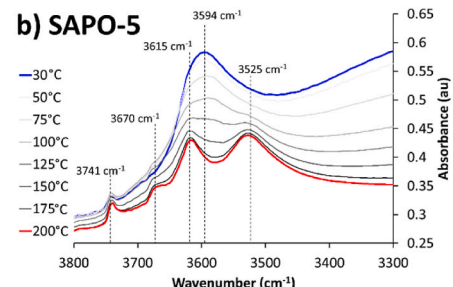
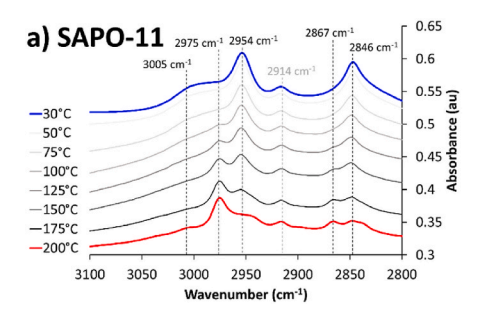


Fig. 3. Operando DRIFTS data of SAPO-5 during the catalytic methanol dehydration to DME process, focussing on the low temperature (\leq 200 °C) regime, with emphasis on the: a) C-H region (3100–2800 cm⁻¹) and b) O-H region (3800–3300 cm⁻¹).



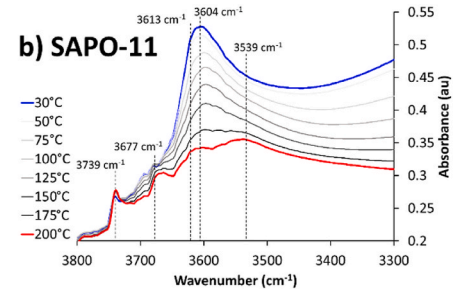


Fig. 4. Operando DRIFTS data of SAPO-11 during the catalytic methanol dehydration to DME process, focussing on the low temperature (\leq 200 °C) regime, with emphasis on the: a) C-H region (3100–2800 cm⁻¹), and b) O-H region (3800–3300 cm⁻¹).

have subtly shifted position, but were still present, supporting the strongly bound assignment. Notable features emerged at 2975 and 2867 cm⁻¹, which have previously been attributed to methoxy species, suggesting that a chemical bond has formed between the C₁ species, and the framework itself [43-46]. This species has previously been identified in a wide range of zeolite frameworks, and is suggested to be a key methylating agent in the MTO process [48,49]. Increasing the temperature from 100 to 200 $^{\rm o}$ C showed a complete removal of strongly bound methanol, leaving methoxy species only. Notably, the appearance of the methoxy species coincided with DME appearing in the MS trace, suggesting that either methoxy formation was integral to DME formation, or the DME produced facilitated methoxy formation. Though as methoxy signals appeared as low as 100 $^{\circ}\text{C},$ with no DME formed, in this case we suggest that the methoxy was a precursor to DME formation, not that DME formed the methoxy groups. This finding is in good agreement with previous work on DME formation, studied by continuous flow magic angle spinning NMR [50]. At 200 °C, a feature appears at 2832 cm⁻¹, this has previously been attributed to DME interacting with hydroxyl species in zeolites (Table 1) [43-46]. Heating the SAPOs further to 350 ^oC (Fig. S9a and S9b) resulted in weakening of the methoxy signals, as the quantity of DME in the MS trace also decreased. In this region, a broad band at 3039 cm⁻¹ appeared, assigned to either sp² C-H groups, or protonated DME. Between 250 and 320 °C, propene was the product primarily detected in the MS trace (Fig. S9c), suggesting MTO chemistry was now occurring. As DME formation requires two molecules of methanol, we propose that it was a methoxy species combining with a methanol molecule that lead to DME formation, as DME production diminished with the loss of signals at 2956 and 2852 cm⁻¹ (attributed to strongly bound methanol). As temperature increased, the remaining methoxy species had sufficient energy to undergo the MTO processes, either by activating DME, or through carbene-like chemistry [44], leading to the formation of propene as confirmed by the online MS analysis. We note however, that in none of our spectra did we observe a signal associated with symmetric methyl stretch associated with protonated DME. Despite DFT calculations [51,52] and experimental works [53], suggesting that this would likely occur at 2960-2965 cm⁻¹ [54].

The O-H region (3800–3300 cm⁻¹) also shows similar trends

(Fig. 3b). From 30 to 150 °C there was a noticeable transition from a single peak at 3594 cm⁻¹, back to the two signals at 3525 and 3615 cm⁻¹. Between 150 and 250 °C, the O-H region was largely unchanged (Fig. 3b & S8b), until eventually there is another increase in the two signals. This was also associated with a decrease in the C-H signals, suggesting that between 250 and 275 °C there was a notable drop in the number of surface methoxy species, which could be attributed to the formation of propene, directly from the methoxy group which is an important step in forming the HCP in MTO chemistry [55,56].

Similar measurements were performed on the other three SAPO systems to probe the differences in reactivity. SAPO-11 (Fig. 4 & S9) showed very similar signals to SAPO-5, though notably SAPO-11 had consistent signals at 2911 cm⁻¹ and 2847 cm⁻¹ (Fig. 4a), which were both present in the dried, bare SAPO-11 spectra. The latter signal however clearly overlapped with strongly bound methanol. SAPO-11 still showed a progression from "bound" methanol (2846 cm⁻¹ and 2952 cm⁻¹) to the methoxy species (2975 cm⁻¹ and 2865 cm⁻¹) [43–46]. Like SAPO-5, the weakly bound methanol (2995 cm⁻¹) signal has greatly diminished by 100 °C. In stark contrast to SAPO-5, signals due to strongly bound methanol remained until 250 °C (Fig. S9a and S9b), which correlated directly with DME being produced over a wider temperature range over SAPO-11, compared to SAPO-5. This was accompanied by the signal at 2832 cm⁻¹ (attributed to bound DME) existing at higher temperatures in SAPO-11 and together provides further evidence that DME was formed by a methoxy species combining with "bound" methanol. In SAPO-5, the intensity of the methoxy signals surpassed bound methanol at 125 °C, whereas in SAPO-11, this did not occur until 175 °C, suggesting that the weaker SAPO-11 acid sites were not as effective at forming methoxy species. In the C-H region, SAPO-11 does not show any notable features around 3035 cm⁻¹. Given that signals due to H-bound DME were present (2832 cm⁻¹), this suggests the BAS in SAPO-11 may not be strong enough to fully protonate DME. MS findings (Fig. S9c) further show that even at temperatures above 330 °C, there was no significant propene formation, which highlighted the influence of the weaker BAS. The O-H region of SAPO-11 (Fig. 4b & S9b) simply showed a smooth progression from hydrogen bonded BAS to reformed BAS, showing the removal of hydrocarbon, oxygen-containing

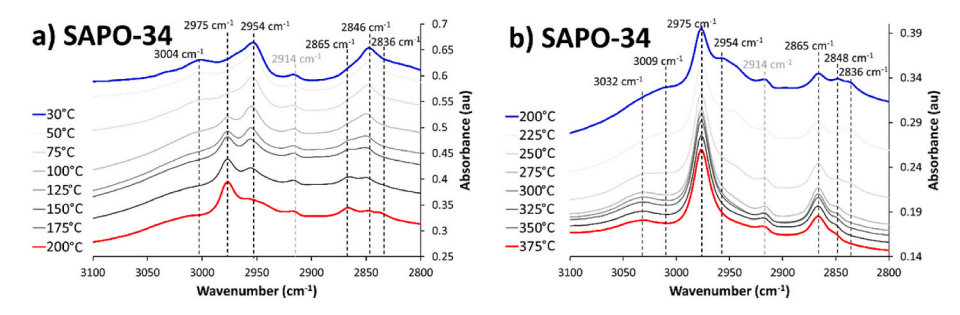


Fig. 5. Operando DRIFTS data of SAPO-34 during the catalytic methanol dehydration to DME process, focussing on the C-H region (3100–2800 cm⁻¹), with emphasis on the: a) low temperature (30–200 °C) regime and b) high temperature (200–375 °C) regime.

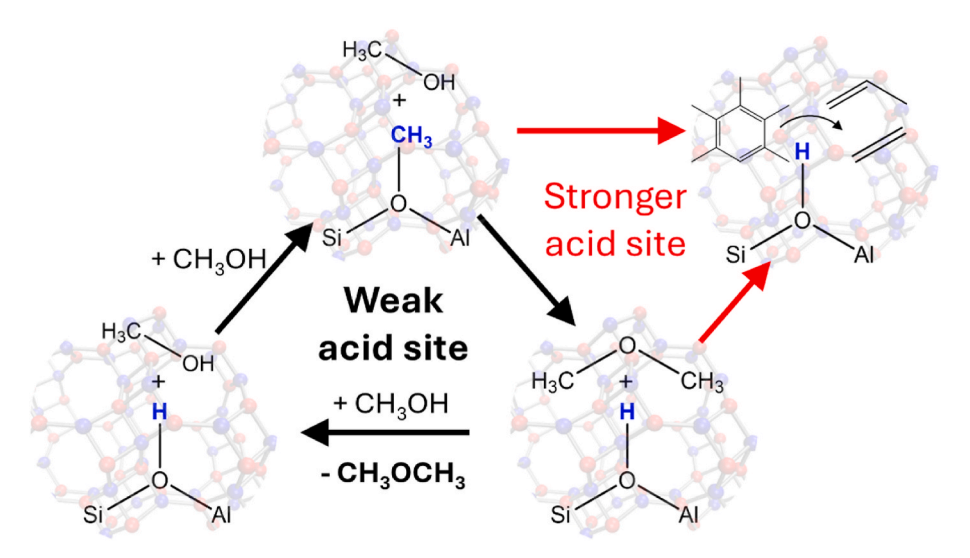


Fig. 6. Proposed mechanism for DME formation and MTO chemistry.

species from SAPO-11, whereas SAPO-5 showed defined regions. This is likely because, whilst the weaker acid sites of SAPO-11 required higher temperatures to form methoxy species, higher temperatures were also required to completely remove them.

Despite significantly better catalytic performance, SAPO-18 (Fig. S10) behaved very similarly to SAPO-11 under operando DRIFTS conditions. Deviations are expected given the disparity between the catalytic conditions and the DRIFTS study. SAPO-34 possessing the largest quantity of stronger BAS and behaved similarly to SAPO-5 (Fig. 5 & S11), forming methoxy species at low temperatures, as shown by the emergence of peaks at 2975 cm⁻¹ and 2867 cm⁻¹ below 100 °C (Fig. 5a). In contrast to SAPO-5, SAPO-34 retained the bound methanol signals (2952 cm⁻¹ and 2852 cm⁻¹) at higher temperatures. In SAPO-5, these signals have disappeared by 200 °C, whereas in SAPO-34, they were still visible (Fig. 5b). This suggests that interactions between non-methoxy methanol species were stronger in SAPO-34 than in SAPO-5, likely due to the stronger BAS in SAPO-34. This could also be due to diffusion of small hydrocarbons being more hindered in the smaller CHA cage of SAPO-34, compared to the larger AFI channels in SAPO-5, as shown previously in works on larger alcohols [57]. As such methanol may be less able to diffuse away from the active site, leading to stronger interactions. This translated to SAPO-34 being able to form both DME and propene (via MTO) over a much wider temperature range (Fig. S11c); SAPO-5 showed no real signs of activity beyond 350 °C, whereas SAPO-34 was still active. This may be partially due to the difference in framework topology. SAPO-5 framework is composed of large cylindrical pores which hinder molecular diffusion less compared to SAPO-34, in which the 3.8 \times 3.8 Å pore windows limit facile diffusion through the framework, thus retaining reactant molecules closer to the acidic active sites and hence potentially improving reactivity in SAPO-34 [40]. At approximately 250 °C, SAPO-34 showed minimal signs of bound methanol, with the remaining signals attributed to methoxy groups, artifacts, or protonated DME (3032 cm⁻¹). The latter signal was much more pronounced than in the other frameworks, which highlighted the ability of SAPO-34 to activate DME, making it a superior

Overall, the DRIFTS study clearly highlighted the importance of methoxy species formation on DME activity, and the need to combine this methoxy group with nearby bound methanol molecules to selectively form DME. This favourable situation can be promoted using weak acid sites, such as those in SAPO-11. In this case, methoxy formation is slowed, leading to a mixture of bound methanol and methoxy species which co-exist in proximity to one another inside the microporous framework (Fig. 6). Moreover, the weaker BAS are less able to initiate

the MTO reaction, by either protonated DME, or carbene-like chemistry to stimulate the HCP mechanism. As such, the weaker BAS can selectively form DME, even at elevated reaction temperatures.

4. Conclusions

This study demonstrated that SAPO-11 uniquely formed weaker BAS compared to SAPO-5, SAPO-18, and SAPO-34. When applied for the methanol dehydration reaction, this resulted in a lower propensity for the popular MTO process, as commonly seen in SAPO-34, instead leading to the selective formation of DME. The inability of SAPO-11 to initiate the MTO process led to limited build-up of aromatic or coke products, drastically increasing longevity and DME selectivity, even at elevated temperatures. Our operando DRIFTS study, in which the CH and OH regions were simultaneously studied with concurrent online MS analysis, showed the importance of combining methoxy species with bound methanol to form DME. While solid acid catalysts such as SAPO-5 and SAPO-34 rapidly desorbed bound methanol, and facilitated the MTO reaction, SAPO-11 retained both the methoxy and bound methanol species, leading to effective DME production with minimal formation of unsaturated species. The catalytic longevity and selectivity of SAPO-11 makes it an attractive candidate for the sustainable production of DME which can aid transitioning the transport sector towards carbon neutrality.

CRediT authorship contribution statement

M.G. Walerowski: Writing – review & editing, Writing – original draft, Validation, Investigation, Formal analysis. A.E. Oakley: Investigation. M. Carravetta: Supervision, Resources, Formal analysis. R. Raja: Supervision, Resources, Project administration, Funding acquisition. L.M. Armstrong: Supervision, Resources, Project administration, Funding acquisition, Conceptualization. M.E. Potter: Writing – review & editing, Writing – original draft, Visualization, Validation, Supervision, Resources, Project administration, Methodology, Investigation, Formal analysis, Data curation.

Declaration of competing interest

The authors declare the following financial interest/personal relationships which may be considered as potential competing interests: Maciej Walerowski reports financial support was provided by the Southampton Marine and Maritime Institute. Matthew Potter reports equipment access was provided through the UK Catalysis Hub, at the

Research Complex at Harwell. The other authors have no known competing financial interests or personal relationships that could have appeared to influence the work reported in this paper.

Acknowledgement

This work was supported by the University of Southampton and the Southampton Marine and Maritime Institute. This work was performed using resources from the UK Catalysis Hub, which was funded by current EPSRC grants: EP/R026939/1 and EP/R026815/1, and who are gratefully acknowledged.

Appendix. A Supplementary data

Supplementary data to this article can be found online at https://doi.org/10.1016/j.micromeso.2025.113783.

Data availability

Data will be made available on request.

References

- J. Sun, G. Yang, Y. Yoneyama, N. Tsubaki, Catalysis chemistry of dimethyl ether synthesis, ACS Catal. 4 (2014) 3346–3356, https://doi.org/10.1021/cs500967j.
- [2] G.A. Olah, A. Goeppert, G.K. Prakash, Chemical recycling of carbon dioxide to methanol and dimethyl ether: from greenhouse gas to renewable, environmentally carbon neutral fuels and synthetic hydrocarbons, J. Org. Chem. 74 (2009) 487-498. https://doi.org/10.1021/ji8801260f.
- [3] A. Alvarez, A. Bansode, A. Urakawa, A.V. Bavykina, T.A. Wezendonk, M. Makkee, J. Gascon, F. Kapteijn, Challenges in the greener production of formates/formic acid, methanol, and DME by heterogeneously catalyzed CO₂ hydrogenation processes, Chem. Rev. 117 (2017) 9804–9838, https://doi.org/10.1021/acs.chemrev.6b00816.
- [4] Z. Azizi, M. Rezaeimanesh, T. Tohidian, M.R. Rahimpour, Dimethyl ether: a review of technologies and production challenges, Chem. Eng. Process. Process Intensif. 82 (2014) 150–172, https://doi.org/10.1016/j.cep.2014.06.007.
- [5] A. Ghosh, D. Nag, R. Chatterjee, A. Singha, P.S. Dash, B. Choudhury, A. Bhaumik, CO₂ to dimethyl ether (DME): structural and functional insights of hybrid catalysts, Catal. Sci. Technol. 14 (2024) 1387–1427, https://doi.org/10.1039/D3CY01497E.
- [6] B. Hamed, A. Chad, Development of heterogeneous catalysts for dehydration of methanol to dimethyl ether: a review, Catalogue Index 11 (2019) 7–33, https:// doi.org/10.1134/S2070050419010045.
- [7] M.E. Potter, L.-M. Armstrong, R. Raja, Combining catalysis and computational fluid dynamics towards improved process design for ethanol dehydration, Catal. Sci. Technol. 8 (2018) 6163–6172, https://doi.org/10.1039/C8CY01564C.
- [8] P. Yan, H. Peng, J. Vogrin, H. Rabiee, Z. Zhu, Selective CO₂ hydrogenation over zeolite-based catalysts for targeted high-value products, J. Mater. Chem. A 11 (2023) 17938–17960, https://doi.org/10.1039/D3TA03150K.
- [9] U. Olsbye, S. Svelle, M. Bjorgen, P. Beato, T.V. Janssens, F. Joensen, S. Bordiga, K. P. Lillerud, Conversion of methanol to hydrocarbons: how zeolite cavity and pore size controls product selectivity, Angew. Chem. Int. Ed. Engl. 51 (2012) 5810–5831, https://doi.org/10.1002/anie.201103657.
- [10] J. Chen, P.A. Wright, J.M. Thomas, S. Natarajan, L. Marchese, S.M. Bradley, G. Sankar, C.R.A. Catlow, P.L. Gai-Boyes, SAPO-18 catalysts and their broensted acid sites, J. Phys. Chem. 98 (2002) 10216–10224, https://doi.org/10.1021/ i100091a042
- [11] M.E. Potter, Down the microporous rabbit hole of silicoaluminophosphates: recent developments on synthesis, characterization, and catalytic applications, ACS Catal. 10 (2020) 9758–9789, https://doi.org/10.1021/acscatal.0c02278.
- [12] J. Chen, P.A. Wright, S. Natarajan, J.M. Thomas, Understanding the brønsted acidity of Sapo-5, Sapo-17, Sapo-18 and SAPO-34 and their catalytic performance for methanol conversion to hydrocarbons, Stud. Surf. Sci. Catal. 84 (1994) 1731–1738, https://doi.org/10.1016/S0167-2991(08)63726-X.
- [13] W. Dai, W. Kong, G. Wu, N. Li, L. Li, N. Guan, Catalytic dehydration of methanol to dimethyl ether over aluminophosphate and silico-aluminophosphate molecular sieves, Catal. Commun. 12 (2011) 535–538, https://doi.org/10.1016/j. catcom.2010.11.019.
- [14] K.S. Yoo, J.-H. Kim, M.-J. Park, S.-J. Kim, O.-S. Joo, K.-D. Jung, Influence of solid acid catalyst on DME production directly from synthesis gas over the admixed catalyst of Cu/ZnO/Al₂O₃ and various SAPO catalysts, Appl. Catal. A: Gen. 330 (2007) 57–62, https://doi.org/10.1016/j.apcata.2007.07.007.
- [15] A.A. Arvidsson, P.N. Plessow, F. Studt, A. Hellman, Influence of acidity on the Methanol-to-DME reaction in zeotypes: a first principles-based microkinetic study, J. Phys. Chem. C 124 (2020) 14658–14663, https://doi.org/10.1021/acs. ipcc.0c03125
- [16] A. Sierraalta, R. Añez, D.S. Coll, P. Alejos, Conversion of methanol to dimethyl ether over silicoaluminophosphates: isolated acid sites and the influence of silicon

- islands. A DFT-ONIOM study, Microporous Mesoporous Mater. 292 (2020) 109732, https://doi.org/10.1016/j.micromeso.2019.109732.
- [17] J.M. Campelo, F. Lafont, J.M. Marinas, M. Ojeda, Studies of catalyst deactivation in methanol conversion with high, medium and small pore silicoaluminophosphates, Appl. Catal. A: Gen. 192 (2000) 85–96, https://doi.org/10.1016/S0926-860X(99) 00329-4
- [18] K.-H. Schnabel, R. Fricke, I. Girnus, E. Jahn, E. Löffler, B. Parlitz, C. Peuker, Catalytic and infrared spectroscopic investigations of the molecular sieve types SAPO-34 and SAPO-11, J. Chem. Soc., Faraday Trans. 87 (1991) 3569–3574, https://doi.org/10.1039/FT9918703569.
- [19] S. Lin, Y. Zhi, W. Chen, H. Li, W. Zhang, C. Lou, X. Wu, S. Zeng, S. Xu, J. Xiao, A. Zheng, Y. Wei, Z. Liu, Molecular routes of dynamic autocatalysis for methanol-to-hydrocarbons reaction, J. Am. Chem. Soc. 143 (2021) 12038–12052, https://doi.org/10.1021/jacs.1c03475.
- [20] W. Dai, X. Wang, G. Wu, N. Guan, M. Hunger, L. Li, Methanol-to-Olefin conversion on silicoaluminophosphate catalysts: effect of brønsted acid sites and framework structures, ACS Catal. 1 (2011) 292–299, https://doi.org/10.1021/cs200016u.
- [21] E. Borodina, H. Sharbini Harun Kamaluddin, F. Meirer, M. Mokhtar, A.M. Asiri, S. A. Al-Thabaiti, S.N. Basahel, J. Ruiz-Martinez, B.M. Weckhuysen, Influence of the reaction temperature on the nature of the active and deactivating species during methanol-to-olefins conversion over H-SAPO-34, ACS Catal. 7 (2017) 5268–5281, https://doi.org/10.1021/acscatal.7b01497.
- [22] J. Goetze, F. Meirer, I. Yarulina, J. Gascon, F. Kapteijn, J. Ruiz-Martinez, B. M. Weckhuysen, Insights into the activity and deactivation of the methanol-to-olefins process over different small-pore zeolites as studied with operando UV-vis spectroscopy, ACS Catal. 7 (2017) 4033–4046, https://doi.org/10.1021/acscatal.6b03677.
- [23] M.E. Potter, S.V. Aswegen, E.K. Gibson, I.P. Silverwood, R. Raja, Spectroscopic investigation into the design of solid-acid catalysts for the low temperature dehydration of ethanol, Phys. Chem. Chem. Phys. 18 (2016) 17303–17310, https://doi.org/10.1039/C6CP01209D.
- [24] M. Calligaris, G. Nardin, L. Randaccio, Cation site location in hydrated chabazites. Crystal structure of potassium- and silver- exchanged chabazites, Zeolites 3 (1983) 205–208, https://doi.org/10.1016/0144-2449(83)90008-8.
- [25] S. Qiu, W. Pang, H. Kessler, J.-L. Guth, Synthesis and structure of the [AlPO₄]₁₂ Pr₄NF molecular sieve with AFI structure, Zeolites 9 (1989) 440–444, https://doi. org/10.1016/0144-2449(89)90101-2.
- [26] J.W. Richardson, J.J. Pluth, J.V. Smith, Rietveld profile analysis of calcined AlPO₄-11 using pulsed neutron powder diffraction, Acta Crystallogr. B. Struct. Sci. 44 (1988) 367–373, https://doi.org/10.1107/S0108768188003076.
- [27] A. Simmen, L.B. McCusker, C. Baerlocher, W.M. Meier, The structure determination and rietveld refinement of the aluminophosphate AIPO₄-18, Zeolites 11 (1991) 654–661, https://doi.org/10.1016/S0144-2449(05)80167-8.
- [28] M.R. Agliullin, Y.G. Kolyagin, D.V. Serebrennikov, N.G. Grigor'eva, A. S. Dmitrenok, V.N. Maistrenko, E. Dib, S. Mintova, B.I. Kutepov, Acid properties and morphology of SAPO-11 molecular sieve controlled by silica source, Microporous Mesoporous Mater. 338 (2022) 111962, https://doi.org/10.1016/j.micromeso.2022.111962.
- [29] D.S. Wragg, D. Akporiaye, H. Fjellvåg, Direct observation of catalyst behaviour under real working conditions with X-ray diffraction: comparing SAPO-18 and SAPO-34 methanol to olefin catalysts, J. Catal. 279 (2011) 397–402, https://doi. org/10.1016/j.jcat.2011.02.011.
- [30] A.S. Makova, V.N. Panchenko, V.A. Bolotov, N.A. Davshan, I.V. Mishin, M. N. Timofeeva, K.I. Shefer, M. Ter-Akopyan, L.M. Kustov, S.H. Jhung, Microwave-assisted synthesis of solketal from glycerol and acetone in the presence of SAPO-34 and SAPO-5, Microporous Mesoporous Mater. 381 (2025) 113361, https://doi.org/10.1016/j.micromeso.2024.113361.
- [31] Y. Huang, Z. Yan, R. Richer, Characterization of BAPO- and SAPO-based mesoporous materials by solid-state NMR spectroscopy, Chem. Mater. 17 (2005) 6545–6554, https://doi.org/10.1021/cm050396j.
- [32] G. Engelhardt, Multinuclear solid-state NMR in silicate and zeolite chemistry, TrAC, Trends Anal. Chem. 8 (1989) 343–347, https://doi.org/10.1016/0165-9936 (89)87043-8
- [33] E. Lippmaa, M. Maegi, A. Samoson, G. Engelhardt, A.R. Grimmer, Structural studies of silicates by solid-state high-resolution silicon-29 NMR, J. Am. Chem. Soc. 102 (2002) 4889–4893, https://doi.org/10.1021/ja00535a008.
- [34] B. Arstad, A. Lind, J.H. Cavka, K. Thorshaug, D. Akporiaye, D. Wragg, H. Fjellvåg, A. Grønvold, T. Fuglerud, Structural changes in SAPO-34 due to hydrothermal treatment. A NMR, XRD, and DRIFTS study, Microporous Mesoporous Mater. 225 (2016) 421–431, https://doi.org/10.1016/j.micromeso.2016.01.024.
- [35] E. Campbell, I.V. Sazanovich, M. Towrie, M.J. Watson, I. Lezcano-Gonzalez, A. M. Beale, Methanol-to-Olefins studied by UV Raman spectroscopy as compared to visible wavelength: capitalization on resonance enhancement, J. Phys. Chem. Lett. 15 (2024) 6826–6834, https://doi.org/10.1021/acs.jpclett.4e00865.
- [36] I. Lezcano-Gonzalez, E. Campbell, A.E.J. Hoffman, M. Bocus, I.V. Sazanovich, M. Towrie, M. Agote-Aran, E.K. Gibson, A. Greenaway, K. De Wispelaere, V. Van Speybroeck, A.M. Beale, Insight into the effects of confined hydrocarbon species on the lifetime of methanol conversion catalysts, Nat. Mater. 19 (2020) 1081–1087, https://doi.org/10.1038/s41563-020-0800-y.
- [37] M.G. Walerowski, S. Kyrimis, M.E. Potter, A.E. Oakley, M. Carravetta, L.-M. Armstrong, R. Raja, Experimental and computational optimisation of methanol dehydration to dimethyl ether, Catal. Sci. Technol. 15 (2025) 3216–3225, https:// doi.org/10.1039/D5CY00062A.
- [38] P. Liu, J. Han, L. Ling, X. Shen, P. Liu, R. Zhang, B. Wang, Correlation of Brønsted acid strengths and species substituted Si in ZSM-5 and their effects on propylene

- polymerization in MTA reaction, Microporous Mesoporous Mater. 347 (2023) 112346, https://doi.org/10.1016/j.micromeso.2022.112346.
- [39] S. Fan, H. Wang, P. Wang, W. Jiao, S. Wang, Z. Qin, M. Dong, J. Wang, W. Fan, Formation and evolution of the coke precursors on the zeolite catalyst in the conversion of methanol to olefins, Chem Catal. 4 (2024) 100927, https://doi.org/ 10.1016/j.checat.2024.100927.
- [40] M.E. Potter, J. Kezina, R. Bounds, M. Carravetta, T.M. Mezza, R. Raja, Investigating the role of framework topology and accessible active sites in silicoaluminophosphates for modulating acid-catalysis, Catal. Sci. Technol. 8 (2018) 5155–5164, https://doi.org/10.1039/C8CY01370E.
- [41] K. Hemelsoet, A. Ghysels, D. Mores, K. De Wispelaere, V. Van Speybroeck, B. M. Weckhuysen, M. Waroquier, Experimental and theoretical IR study of methanol and ethanol conversion over H-SAPO-34, Catal. Today 177 (2011) 12–24, https://doi.org/10.1016/j.cattod.2011.05.040.
- [42] L. Wang, W. Li, S.J. Schmieg, D. Weng, Role of Brønsted acidity in NH₃ selective catalytic reduction reaction on Cu/SAPO-34 catalysts, J. Catal. 324 (2015) 98–106, https://doi.org/10.1016/j.jcat.2015.01.011.
- [43] T.R. Forester, R.F. Howe, In situ FTIR studies of methanol and dimethyl ether in ZSM-5, J. Am. Chem. Soc. 109 (1987) 5076–5082, https://doi.org/10.1021/ io00251-004
- [44] I.B. Minova, M. Bühl, S.K. Matam, C.R.A. Catlow, M.D. Frogley, G. Cinque, P. A. Wright, R.F. Howe, Carbene-like reactivity of methoxy groups in a single crystal SAPO-34 MTO catalyst, Catal. Sci. Technol. 12 (2022) 2289–2305, https://doi.org/10.1039/D1CY02361F
- [45] J.W. Park, G. Seo, IR study on methanol-to-olefin reaction over zeolites with different pore structures and acidities, Appl. Catal. A: Gen. 356 (2009) 180–188, https://doi.org/10.1016/j.apcata.2009.01.001.
- [46] M. Rep, A.E. Palomares, G. Eder-Mirth, J.G. van Ommen, N. Rösch, J.A. Lercher, Interaction of methanol with alkali metal exchanged molecular sieves. 1. IR spectroscopic study, J. Phys. Chem. B 104 (2000) 8624–8630, https://doi.org/ 10.1021/jp0001945.
- [47] L. Lin, M. Fan, A.M. Sheveleva, X. Han, Z. Tang, J.H. Carter, I. da Silva, C.M. A. Parlett, F. Tuna, E.J.L. McInnes, G. Sastre, S. Rudic, H. Cavaye, S.F. Parker, Y. Cheng, L.L. Daemen, A.J. Ramirez-Cuesta, M.P. Attfield, Y. Liu, C.C. Tang, B. Han, S. Yang, Control of zeolite microenvironment for propene synthesis from methanol, Nat. Commun. 12 (2021) 822, https://doi.org/10.1038/s41467-021-21062-1.

- [48] R.Y. Brogaard, R. Henry, Y. Schuurman, A.J. Medford, P.G. Moses, P. Beato, S. Svelle, J.K. Nørskov, U. Olsbye, Methanol-to-hydrocarbons conversion: the alkene methylation pathway, J. Catal. 314 (2014) 159–169, https://doi.org/ 10.1016/i.jcat.2014.04.006.
- [49] Y. Chen, S. Wang, Z. Wei, J. Li, M. Dong, Z. Qin, J. Wang, W. Fan, Unraveling the relationship between zeolite structure and MTO product distribution by theoretical study of the reaction mechanism, J. Phys. Chem. C 125 (2021) 26472–26483, https://doi.org/10.1021/acs.jpcc.1c07692.
- [50] W. Wang, M. Seiler, M. Hunger, Role of surface methoxy species in the conversion of methanol to dimethyl ether on acidic zeolites investigated by in situ stoppedflow MAS NMR spectroscopy, J. Phys. Chem. B 105 (2001) 12553–12558, https:// doi.org/10.1021/jp0129784.
- [51] S.A.F. Nastase, C.R.A. Catlow, A.J. Logsdail, QM/MM study of the stability of dimethyl ether in zeolites H-ZSM-5 and H-Y, Phys. Chem. Chem. Phys. 23 (2021) 2088–2096, https://doi.org/10.1039/D0CP05392A.
- [52] P.G. Moses, J.K. Nørskov, Methanol to dimethyl ether over ZSM-22: a periodic density functional theory study, ACS Catal. 3 (2013) 735–745, https://doi.org/ 10.1021/cs300722w
- [53] T. Omojola, N. Cherkasov, A.I. McNab, D.B. Lukyanov, J.A. Anderson, E.V. Rebrov, A.C. van Veen, Mechanistic insights into the desorption of methanol and dimethyl ether over ZSM-5 catalysts, Catal. Lett. 148 (2017) 474–488, https://doi.org/ 10.1007/s10562-017-2249-4.
- [54] S. Wang, Z. Qin, M. Dong, J. Wang, W. Fan, Recent progress on MTO reaction mechanisms and regulation of acid site distribution in the zeolite framework, Chem Catal. 2 (2022) 1657–1685, https://doi.org/10.1016/j.checat.2022.05.012.
- [55] H. Yamazaki, H. Shima, H. Imai, T. Yokoi, T. Tatsumi, J.N. Kondo, Direct production of propene from methoxy species and dimethyl ether over H-ZSM-5, J. Phys. Chem. C 116 (2012) 24091–24097, https://doi.org/10.1021/jp307290z
- [56] J. Li, Z. Wei, Y. Chen, B. Jing, Y. He, M. Dong, H. Jiao, X. Li, Z. Qin, J. Wang, W. Fan, A route to form initial hydrocarbon pool species in methanol conversion to olefins over zeolites, J. Catal. 317 (2014) 277–283, https://doi.org/10.1016/j. icat.2014.05.015.
- [57] M.E. Potter, J. Amsler, L. Spiske, P.N. Plessow, T. Asare, M. Carravetta, R. Raja, P. A. Cox, F. Studt, L.-M. Armstrong, Combining theoretical and experimental methods to probe confinement within microporous solid acid catalysts for alcohol dehydration, ACS Catal. 13 (2023) 5955–5968, https://doi.org/10.1021/acscatal.3c00352.